Article

Hybrid Magnetic Hydrogel: A Potential System for Controlled Drug Delivery by Means of Alternating Magnetic Fields

Gabriele Giani, Serena Fedi and Rolando Barbucci *

Centro Interuniversitario Sistemi Medici Avanzati (C.R.I.S.M.A.), Colle di Val d'Elsa Viale Matteotti 15, Siena, 53034 Colle di Val d'Elsa, Italy; E-Mails: gabriele1485@gmail.com (G.G.); fedi6@unisi.it (S.F.)

* Author to whom correspondence should be addressed; E-Mail: rolando.barbucci@unisi.it; Tel.: +39-0577-900327; Fax: +39-0577-900322.

Abstract: Novel hybrid magnetic hydrogels have demonstrated their influence in several areas, particularly in biomedical science where these innovative materials are showing interesting applications for controlled drug delivery. A hybrid hydrogel with $CoFe_2O_4$ nanoparticles (NPs) as cross-linker agents of carboxymethylcellulose (CMC) polymer was obtained with the aim of testing it as a system for controlled drug release. The NPs were functionalized with (3-aminopropyl)-trimethoxysilane (APTMS) in order to introduce-NH_2 groups on the surface. Infrared spectroscopy, XPS and electrochemical analysis were performed to quantify the amino coating. The presence of magnetic nanoparticles makes the system suitable for an application with magnetic stimulus. Preliminary studies performed with alternating magnetic fields indicate a release of the drug-like molecules previously loaded in the matrix.

1. Introduction

Hydrogels can be defined as cross-linked polymer networks which can absorb large amounts of water or biological fluids [1]. Hydrogels are currently being considered for various biological applications such as components of drug delivery devices, microfluidic devices, biosensors, tissue implants and contact lenses [1,2]. Unique properties can be achieved by incorporating various

nano- and micro-scale materials such as metal particles into the hydrogel matrix [3]. Recently, materials with magnetic nanoparticles inserted into them have been prepared and studied for numerous technological and biomedical applications, including tissue engineering, magnetic separation, MRI contrast agents, hyperthermia and thermal ablation [4–6]. One of the most promising applications for magnetic nanoparticles is in the field of the drug release, especially for cancer therapy. This innovative strategy for targeted drug delivery consists of coupling the drug to magnetic nanoparticles (NPs) that can be guided to the target by means of external magnetic fields [7,8]. Once they reach the target, the NPs release the drugs under the influence of an alternate magnetic field. The main drawbacks of NPs are related to the small amount of drug that can be linked to each NP, the possibility of drug deactivation once it is chemically bound to the NP, and the possibility of its immediate uncontrollable passive release (burst effect) [9]. The former drawback makes it necessary to inject a high concentration of NPs for treatment, with potential systemic toxic effects. Some of these problems can be overcome by introducing magnetic nanoparticles in a hydrogel. The main advantage of the hydrogel is that a larger amount of drug can be loaded, in comparison to that carried by magnetic NPs in dispersion. The presence of magnetic nanoparticles gives the hybrid system the capacity to respond to external magnetic stimulus, such as alternating magnetic fields (AMF), and to localize the hydrogel near the target site through the use of an appropriate magnet [10–14]. So far, different approaches to the utilization of metal oxide nanoparticles in hydrogels have been suggested [15,16]. However, these traditional approaches have many limitations, including the possible release of the NP from the hydrogel matrix into the external environment. One strategy to overcome these problems involves the use of NPs as hydrogel cross-linker agents [12,17].

The aim of this study is to obtain a polysaccharide magnetic hybrid hydrogel capable of serving as a system for the release of a drug (or a model of drug) by means of the application of AMF. The organic part consists of a carboxymethylcellulose (CMC) polymer, while the inorganic part is made up of $CoFe_2O_4$ magnetic NPs. The synthesis strategy involves the formation of a covalent bond between the CMC chains and the magnetic NPs, which act as "cross-linker" agents and allow the formation of a hydrogel.
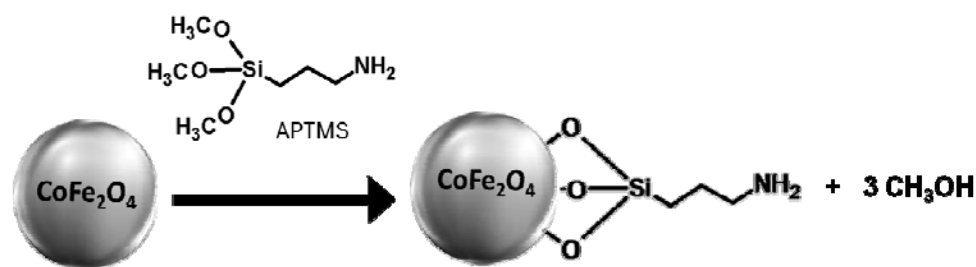
2. Results and Discussion

The formation of a CMC polysaccharide-based hydrogel with functionalized $CoFe_2O_4$ NPs as "cross-linker" agents occurs via four steps.

The first step is the functionalization of the NPs with (3-aminopropyl) trimethoxysilane (APTMS), with the aim of introducing-NH_2 groups onto the metal oxide surface (NP-NH_2). The second step is the sonication of NP-NH_2, to prevent the formation of large aggregates in suspension. The third step is the hybrid hydrogel synthesis by means of reaction of the sonicated suspension of NP-NH_2 and CMC polymer in the presence of activating agents. The fourth step is the loading of the model drug and its release by means of the application of alternating magnetic fields (AMF). These four steps are described in detail below.
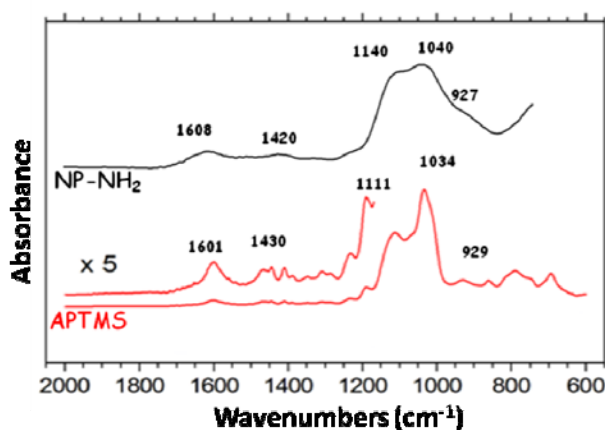
2.1. Functionalized Nanoparticles (NP-NH₂)

In order to bind the NPs to the CMC chains, the nanoparticles are treated with 3-aminopropyltrimethoxysilane (APTMS, Figure1). APTMS hydrolyzes in the presence of water and, in a subsequent reaction, the silanol groups condensate with the hydroxyl groups on the NPs' surface to form M-O-Si covalent bonds. This method introduces onto the NP surface the amino group essential to create an amide bond with the activated carboxylic group of CMC polymers [12,17].

Figure 1. Schematic representation of the functionalization reaction of (3-aminopropyl)-trimethoxysilane (APTMS) with nanoparticle (NP) surface.
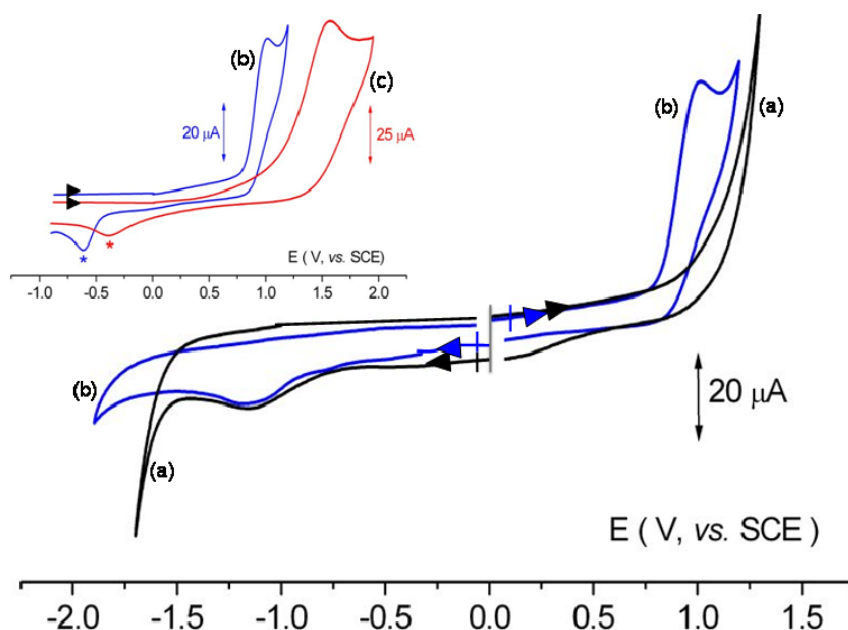

The success of the nanoparticle silanization can be confirmed by infrared analysis. Figure 2 shows APTMS (bottom) and NP-NH₂ (top) FT-IR spectra. Both spectra show common -NH₂ and Si-O absorptions: the bands at ~1,600 and ~1,410 cm^{-1} are assigned to the bending mode of the -NH₂ group and to the scissor vibration of -NH, respectively. The two bands appearing at ~1,100 and ~1,040 cm^{-1}, as well as a somewhat weaker band at ~ 920 cm^{-1}, can be attributed to the vibrational modes involving the bridging oxygen atoms in Si-O-Si and Si-O bonds [18]. Moreover, the XPS spectrum of NP-NH₂ showed the presence of signals at 400 eV and 150 eV, ascribable respectively to the presence of N and Si, absent in the spectrum of bare NPs. This evidence clearly confirms the presence of an aminosilane coating on the surface [12].The XPS study provided an estimated thickness of APTMS on the nanoparticle surface of about 1–2 layers, and showed the presence of many amino active groups on the surface for binding the polysaccharides chains.

Figure 2. FT-IR spectra of APTMS (bottom) and NP-NH₂ (top). Some common absorption confirms the presence of a coating on the surface.

Other information regarding the quantity of NH_2 groups present on NP was obtained by electrochemical analysis of NP, NP-NH_2 and APTMS in DMSO and CH_2Cl_2 solutions. Although the proposed drug delivery systems will be used in an aqueous environment, DMSO and CH_2Cl_2 solvents were employed instead of water because they offer a wider potential window; in an aqueous solution, the processes under study would have been masked by solvent discharge. XPS and IR spectroscopy have investigated the NP in the solid state, while by means of cyclic voltammetry, we look at their solution properties. In Figure 3, the redox behaviors of sonicated NP (a), sonicated NP-NH_2 (b) and APTMS (c) are compared. The NP in DMSO solution undergoes a not-well-defined reduction process at $E_{pc} = -1.17$ V that seems to be an overlapping of several processes; the cathodic potential value and the shape of this peak correspond closely to those found for iron ion reductions in $CoFe_2O_4$ spinel electrodes [19,20].

Figure 3. Cyclic Voltammograms registered on platinum working electrode of (**a**) NP saturated solution after 30'sonication; (**b**) NP-NH_2 0.023 g in 0.020 l after 30'sonication in DMSO solution; and (**c**) APTMS 2.3×10^{-3} mol dm^{-3} in CH_2Cl_2 solution (unfortunately, the corresponding process in DMSO is prevented by solvent discharge). Scan rate 0.20 V sec^{-1}. Supporting electrolyte (**a**) and (**b**): [NEt$_4$][PF$_6$] 0.1 mol dm^{-3}; (**c**): [NBu$_4$][PF$_6$] 0.2 mol dm^{-3}.

APTMS in CH_2Cl_2 solution undergoes an irreversible oxidation process at $E_{pa} = +1.56$ V which is assigned as amine centred [21]. The irreversibility of this process means that the oxidation process causes APTMS decomposition and generates a by-product which reduces at $E_p = -0.40$ V (asterisked peak).

NP-NH_2 cyclic voltammogram in DMSO solution shows both an irreversible cathodic process at $E_{pc} = -1.17$ V and an irreversible anodic process at $E_{pa} = +1.02$ V that generates a by-product ($E_p = -0.61$ V) (asterisked peak). The reduction process is identical to that found in NP cyclic voltammetry. As shown in the insert in Figure 3, the oxidation process of NP-NH_2 in DMSO and that of APTMS in CH_2Cl_2 show similar anodic pathways and similar by-product formation, so both are

amine oxidation processes, although the anodic potential value of APTMS is 500 mV higher than that of NP-NH$_2$. The NP-NH$_2$'s oxidation shift towards less anodic potentials cannot be explained merely in terms of a different diffusion coefficient, but rather depends on APTMS deposits on the NP surface, and may also depend on the conjugation of the redox-active species with an electron withdrawing group such as the nanoparticle core. The electrochemical study not only confirms the presence of an aminosilane coating on the nanoparticle surface, but most importantly demonstrates that the amino groups are free for successive reactions.

In cyclic voltammetry, the current value of a specific process is proportional to the redoxactive species concentration. This consideration suggests a means for estimating the number of APTMS molecules on the NP surface. The current peak height of 2.3×10^{-3} mol dm^{-3} APTMS in CH$_2$Cl$_2$ solution is 52 ± 6 μA, and that of 0.023 g in 0.020 L of NP-NH$_2$ in DMSO solution is 32 ± 4 μA, so we can therefore calculate a $(1.4 \pm 0.3) \times 10^{-3}$ mol dm^{-3} concentration of NH$_2$ groups in NP-NH$_2$ solution. With an average particle size of 60 nm measured by AFM (as discussed in the next paragraph) and a cobalt ferrite density of 5.15 g cm^{-3}, we can further estimate that the number of APTMS molecules bonded to the surface was about $(4 \pm 1) \times 10^5$ per nanoparticle. (assuming spherical nanoparticles and negligible aminosilane coating contribution to nanoparticle density). Moreover, for a typical Si-O bond length of 0.16 nm, it is possible to calculate a thickness of APTMS on the nanoparticle surface of about 2.5 ± 0.5 layers, very close to XPS and the literature data [22–26].

2.2. Sonication of NP-NH$_2$

Synthesis of the hybrid hydrogel requires a uniform distribution of the nanoparticles—The cross-linker agents-in the reaction mixture. Figure 4 shows the dispersions of bare (left) and silanized (right) nanoparticles. The instability of bare nanoparticles, which tend to aggregate and sediment, is clearly evident. The introduction of a coating of silane molecules on the surface prevents the agglomeration and makes for a more stable suspension [27,28]. As previously reported, one factor that may influence the dimension of the aggregates is sonication [29,30]. This effect in NP-NH$_2$ dispersion is depicted in the AFM images in Figure 5.
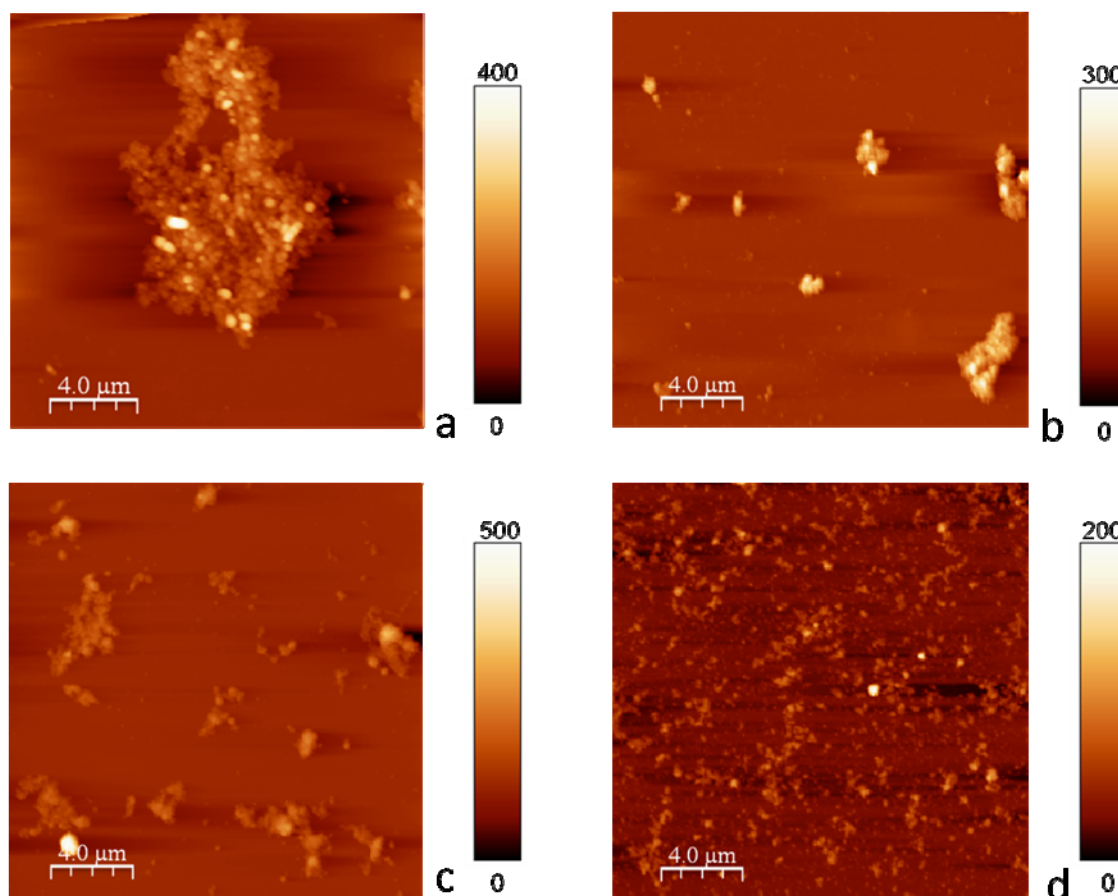
Figure 4. Bare (left suspension) and silanized (right suspension) images of CoFe$_2$O$_4$ nanoparticles (0.02 mg/mL, pH 4). The instability of bare nanoparticles is clearly evident.

Figure 5 shows the morphology of bare nanoparticles (a); unsonicated silanized suspension (b); and silanized suspension sonicated for two different time periods (c = 5 minutes, d = 45 minutes). The images clearly indicate the formation of large aggregates, which explain the instability of the

suspension reported in Figure4. Figure 5b shows silanized nanoparticles without sonication; here, there are fewer aggregates of smaller dimensions than bare nanoparticles. In Figure 5c, the suspension after 5 minutes of sonication shows smaller nanoparticle dimension and a better dispersion. The same trend is shown in Figure 5d (45 minutes of sonication), where the absence of aggregates and more uniform NP-NH$_2$ distribution is evident. Moreover, particle dimension and distribution remain unchanged even after an entire day, as determined by further AFM analysis. The average diameter of the more dispersed nanoparticles measured by AFM analysis is 60 nm.

Figure 5. AFM images of different suspensions of NPs. (**a**) bare NPs; (**b**) NP-NH$_2$; (**c**) NP-NH$_2$ sonicated for 5 minutes; (**d**) NP-NH$_2$ sonicated for 45 minutes.

2.3 Hybrid Hydrogel (CMC-NP) Synthesis

The strategy for the synthesis of CMC-NP involves the formation of amide bonds between the carboxylic groups of CMC and the amine groups of the functionalized NPs in the presence of EDC and NHS [12,17]. A schematic diagram of the reaction is shown in Figure 6. EDC reacts with a carboxyl group to form an amine-reactive *O*-acylisourea intermediate, which allows reactions with the primary amine of the NP-NH$_2$.

The CMC-NP hydrogel (Figure7) shows a homogenous coloration, indicating an even distribuition.

Figure 6. Reaction scheme of the formation of carboxymethylcellulose (CMC) hybrid hydrogels. The reaction involves the formation of an amide bond between the carboxylic groups of CMC and the amine groups of the NP-NH$_2$ (the cross-linker agent) in the presence of *N*-(3-dimethylaminopropyl)-*N*-ethylcarbodiimidehydrochloride (EDC) and N-hydroxysuccinimide (NHS).
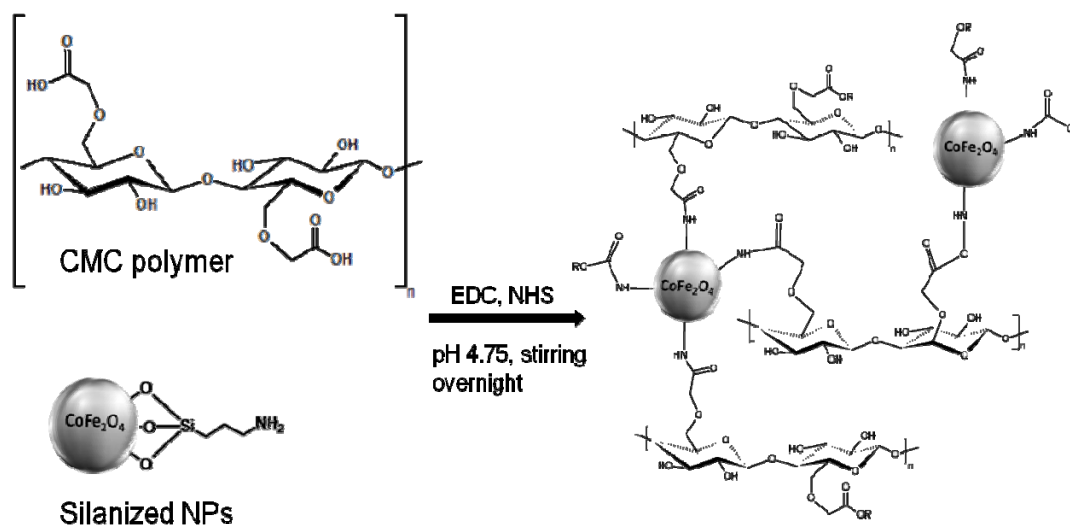

Figure 7. Images of CMC-NP.

The results of the rheological characterizations of CMC-NP were compared with those of the CMC hydrogel cross-linked with 1,3-diaminopropane (CMC-DAP), a bifunctional organic compound used to cross-link polysaccharides without the use of nanoparticles (Table 1) [1]. Stress sweep test analyses were performed to measure the elastic (G') and viscous (G") moduli of the hydrogels samples. The dynamic mechanical analysis indicated a "gel-like" behavior, with the G' greater than the G" within the frequency range analyzed for both the hydrogels. The difference between the elastic modulus for the CMC-NP hydrogel (G' = 3,000 ± 300) and the CMC-DAP hydrogel (G' = 550 ± 100), *i.e.*, the hydrogel obtained crosslinking the CMC chains by 1,3 diamino propane has to be attributed to the presence of NPs in the hydrogel matrix. As for nanocomposite, the enhancement of the above-mentioned properties is strongly dependent on the interactions between filler and polymer. The introduction of an inorganic phase in a hydrogel matrix determines enhanced mechanical proprieties. The increased value of G' can be explained by the good distribution of NP-NH$_2$ that leads to the formation of an ordinate structure, which is reflected in the increased value of the elastic modulus [31,32]. Instead, the loss modulus shows no significant difference between the samples, it means that their viscosity is almost

the same. The viscosity is mainly decided by the continuous phase, which is represented by the CMC hydrogel in both the samples [33].
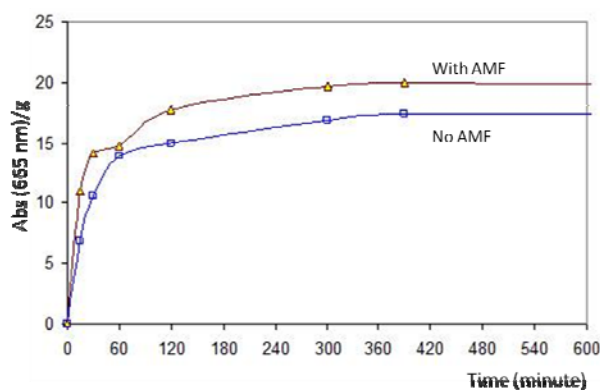
Table 1. G' and G" values for CMC-DAP and CMC-NP.

Sample	G'	G"
CMC-DAP	550 ± 100	60 ± 30
CMC-NP	$3,000 \pm 300$	90 ± 20

2.4. Drug Loading and Drug Release by Means of AMF

In order to verify whether the CMC-NP hydrogel is capable of working as a system for controlled drug release by means of the application of AMF, some samples containing magnetic nanoparticles (0.3 mg) into the lyophilized hydrogel (1 mg) were immersed in a solution containing 2 mg/mL of methylene blue as a drug model. The hydrogel thus loaded with large amounts of drug model turned blue. One set of the loaded hydrogel was placed in a cuvette and left with no exposure to the AMF. A second set of loaded hydrogel was placed in a cuvette, put in the center of the solenoid and continuously subjected to AMF for several hours. Cumulative release of the model drug for both samples was quantified by UV spectrophotometry measuring the absorbance of the diagnostic peak at 665 nm at regular time intervals. The results are shown in Figure 8, where cumulative drug release *vs.* time is plotted for the samples under study. The experimental results show a greater drug release at all time intervals for the sample exposed to AMF than that of the unexposed sample. This improved release is caused by the alignment of the nanoparticles' magnetic moments with that of the external magnetic field, the continuous alteration of which probably leads to the expansion of the hydrogel networks and allows a greater number of methylene blue molecules to leave the gel matrix and enter the medium. No heating effect was observed in our measurements even if the time of AMF applications is rather long (10 hours). The release must depend on a different mechanism than the thermal effect which is reported in literature as being responsible for the delivery of drug for similar systems with free NP inside [10,13,14].

Figure 8. Drug release profile for CMC-NP samples. The red curve is the sample exposed at AMF; blue curve is the sample without AMF. Other measurements performed with different conditions confirm the same trend.

Extensive analyses are in progress to gain further insight into the effects of the alternating magnetic field on drug release, in order to explain the release mechanism.

3. Experimental Section

3.1. Materials

The sodium salt carboxymethylcellulose (CMC, molecular weight: 700 kDa, with a degree of carboxymethylation of 0.86) was supplied by Sigma-Aldrich. Commercial water dispersion of cobalt ferrite NPs was provided by Colorobbia (Italy). The NPs have a $CoFe_2O_4$ stoichiometry. Silane coupling agent 3-aminopropyltrimethoxysilane (APTMS), *N*-hydroxysuccinimide (NHS), *N*-(3-dimethylaminopropyl)-*N*-ethylcarbodiimidehydrochloride (EDC), 1,3-diaminopropane (DAP), and all the reagents were purchased from Sigma-Aldrich.

3.2. Methods

3.2.1. Functionalization of the $CoFe_2O_4$ NPs (NP-NH$_2$)

The NP functionalization reaction was carried out by means of the chemistry of silane molecules, according to the procedure already reported in literature [12,17]. Briefly, 5 mL of (3-aminopropyl)-trimethoxysilane (APTMS), corresponding to a molar ratio of 4.5 relative to the moles of the NPs, were added to a suspension containing 0.5 g of NPs in a 95/5% v/v ethanol/water mixture at pH 5. The functionalized NPs (NP-NH$_2$) were precipitated by centrifugation at 14,000 rpm and washed with ethanol before being dried in a vacuum oven at 45 °C overnight. The NP-NH$_2$ were analyzed by FT-IR, XPS and electrochemistry to verify the presence of APTMS coating on the surface. AFM and analysis was performed to evaluate NP-NH$_2$ aggregation.

3.2.2. Preparation of the Hybrid Hydrogel (CMC-NP)

The CMC hybrid hydrogel containing NP-NH$_2$ was prepared using a procedure already reported in the literature [12,17]. Briefly, 1 g of CMC was first dissolved in deionized water at a concentration of 1.5% w/v. *N*-Hydroxysuccinimide (NHS) and *N*-(3-dimethylaminopropyl)-*N*-ethyl-carbodiimide hydrochloride (EDC) were then added to this solution at a molar ratio of 0.5 relative to the moles of the carboxyl groups of the polysaccharide.

0.5 g of NP-NH$_2$ was added to the mixture and the pH was adjusted to 4.5 with 1 M HCl. Once formed, the hydrogel was purified by washing in water until no traces of EDC or NHS were revealed by UV and FT-IR spectroscopy. A hydrogel was also prepared using 1,3-diaminopropane (DAP) as cross-linker according to a previously described procedure, and was referred to as the control sample (CMC-DAP) [1].

3.2.3. Attenuated Total Reflection Fourier Transform Infrared Spectroscopy (ATR/FT-IR)

The NP-NH$_2$ sample was analyzed dry. ATR spectra of the sample were recorded on a Bio-Rad FTS600 between 4,000 and 750 cm^{-1}. An MCT (mercury-cadmium-tellurium) detector was used and

the apparatus was purged with dry nitrogen. Spectra were averaged at 128 scans at a resolution of 4 cm^{-1} with baseline correction and smoothing, using WIN-IR PRO version 2.6 software.

3.2.4. Electrochemical Measurements

Cyclic voltammetry was performed in a three-electrode cell containing a platinum or gold working electrode surrounded by a platinum-spiral counter electrode, and an aqueous saturated calomel reference electrode (SCE) mounted with a Luggin capillary. A BAS 100W electrochemical analyser was used as the polarising unit. All the potential values refer to the saturated calomel electrode (SCE). Under the present experimental conditions, the one-electron oxidation of ferrocene occurs at E' = +0.39 V in dichloromethane (CH$_2$Cl$_2$) solution and at E' = +0.40 V in dimethylsulfoxid (DMSO) solution. APTMS is a Fluka product and was used as received. NPs and NP-NH$_2$ solutions were sonicated before cyclic voltammogramm registration; unsonicated solutions provided no voltammetric results. Sigma-Aldrich anhydrous 99.8% CH$_2$Cl$_2$ and anhydrous 99.9% DMSO were used as received. Fluka [NBu$_4$][PF$_6$] and [NEt$_4$][PF$_6$] (electrochemical grade) were used as supporting electrolytes.

3.2.5. Atomic Force Microscopy (AFM)

AFM measurements were performed using a Solver-Pro microscope (NT-MDT, Russia).

Aqueous dispersions at pH 4.5 of NP-NH$_2$ at a concentration of 0.02 mg/mL were cast onto freshly cleaved mica, yielding a clean and atomically flat surface. This pH was chosen because it is used during the synthesis of the CMC-NP hydrogels. The nanoparticle samples were kept in an oven until completely dry and analyzed. Images with different scan sizes were acquired in the air in non-contact mode using sharpened silicon tips with spring constants ranging from 2.5 to 10 N m^{-1} and a nominal resonance frequency between 120 and 180 kHz. Data processing was carried out using NTMDT SPM software and WSxM software 5.0.

3.2.6. Rheological Characterization (CMC-NP)

The viscoelastic properties of the gels were assessed by stress sweep test experiments using a rotational rheometer AR2000 Rheometer (TA-Instruments, Leatherhead, UK) in the parallel plate configuration at a controlled temperature of 25 ± 1 °C. In a dynamic experiment, the material was subjected to a sinusoidal shear strain and the mechanical response, expressed as shear stress of viscous-elastic materials, is intermediate between an ideal, pure elastic solid (obeying Hooke's law) and an ideal, pure viscous fluid (obeying Newton's law). The parameters which describe the viscous-elastic behavior are the shear storage modulus G' and the shear loss modulus G'' and are dependent on the oscillation frequency. A frequency of 1 Hz was used. G' provides information about the elasticity or the energy stored in the material during deformation, whereas G'' describes the viscous character or the energy dissipated as heat.

3.2.7. Drug Loading and Drug Release by AMF

Methylene blue (MW 320) was used as the model drug for the controlled drug release demonstration. This molecule has a positive charge like Doxorubicin, a drug used in cancer therapy

and our target molecule for this kind of application. A solution of methylene blue (2 mg/mL) was used to soak the lyophilized CMC-NP hydrogel for 72 h at 25 °C. Subsequently, the release behavior of loaded hydrogel was studied by means of a purpose-built AFM generator with a frequency of 40 KHz and power of 10 W. Final supernatant was collected at 10 h, and cumulative release at different time intervals was quantified by UV—Vis spectrophotometer at 665 nm (Amersham Bioscience).

4. Conclusions

In summary, the method developed in this project suggests a method of preparing hybrid hydrogel with magnetic nanoparticles covalent bound in the matrix.

The hybrid hydrogel combines the magnetic proprieties of $CoFe_2O_4$ nanoparticles and the behaviors typical of hydrogel to create a new system that overcomes some of the drawbacks of NP use in the field of drug release. This new system can be loaded with a large amount of drug and positioned near the target site. Moreover, preliminary results demonstrate the possibility of bringing about the release of drug-like molecules by means of application of magnetic stimulus. This novel, "intelligent" biomaterial and system promises numerous potential applications in terms of drug delivery. Further analysis is underway to better understand factors affecting the drug delivery rate.

References

1. Barbucci, R.; Giardino, R.; de Cagna, M.; Golini, L; Pasqui, D. Inter-Penetrating Hydrogels (IPHs) as a new class of injectable polysaccharide hydrogels with thixotropic nature and interesting mechanical and biological properties. *Soft Matter* **2010**, *6*, 3524–3532.
2. Peppas, N.A. *Hydrogels in Medicine and Pharmacy*; CRC Press: Boca Raton, FL, USA, 1987.
3. Schexnailder, P.J.; Schmidt, G. Nanocomposite hydrogels. *Colloid Polym. Sci.* **2009**, *287*, 1–11.
4. Narayana Reddy, N.; Varaprasad, K.; Subba Reddy, G.V.; Reddy, K.M.S.; Mohan Reddy, K.M.; Mohana Raju, K. Evaluation of blood compatibility and drug release studies of gelatin based magnetic hydrogel nanocomposites. *Colloids Surf. A physicochem. Eng. Asp.* **2011**, *385*, 20–27.
5. Kim, J.; Chun, C.; Kimd, B.; Hong, J.; Cho, J.K. Thermosensitive/magnetic poly(organophosphazene) hydrogel as a long-term magnetic resonance contrast platform. *Biomaterials* **2012**, *33*, 218–222.
6. Meenach, A.; Hilt, Z.; Anderson, W. Poly(ethylene glycol)-based magnetic hydrogel nanocomposites for hyperthermia cancer therapy. *Acta Biomater.* **2010**, *6*, 1039–1046.
7. Gaihre, B.; Khil, S.; Lee, R.; Kim, Y. Gelatin-coated magnetic iron oxide nanoparticles as carrier system: Drug loading and *in vitro* drug release study. *Int. J. Pharm.* **2009**, *365*, 180–189.

8. Drbohlavova, J.; Chomoucka, J.; Huska, D.; Adam, V.; Kizek, R.; Hubalek, J. Magnetic nanoparticles and targeted drug delivering. *Pharmacol. Res.* **2010**, *62*, 144–149.

9. Mahmoudi, M.; Simchi, A.; Hafeli, O.U. Superparamagnetic iron oxide nanoparticles with rigid cross-linked polyethylene glycol fumarate coating for application in imaging and drug delivery. *J. Phys. Chem. C* **2009**, *113*, 8124–8131.

10. Satarkar S.; Hilt, Z. Hydrogel nanocomposites as remote-controlled biomaterials. *Acta Biomater.* **2008**, *4*, 11–16.

11. Satarkar, S.; Hilt, Z. Magnetic hydrogel nanocomposites for remote controlled pulsatile drug release. *J. Control. Release* **2008**, *130*, 246–251.

12. Barbucci, R.; Pasqui, D.; Giani, G.; de Cagna, M.; Fini, M.; Giardino, R.; Atrei, A. A novel strategy for engineering hydrogels with ferromagnetic nanoparticles as crosslinkers of the polymer chains. Potential applications as a targeted drug delivery system. *Soft Matter* **2011**, *7*, 5558–5565.

13. Hu, S.H.; Liu, T.Y.; Liu, D.M.; Chen, Y. Controlled pulsatile drug release from a ferrogelby a high-frequency magnetic field. *Macromolecules* **2007**, *40*, 6786–6788.

14. Brulé, S.; Levy, M.; Wilhelm, C.; Letourneur, D.; Gazeau, F.; Ménager, C.; Le Visage, C. Doxorubicin release triggered by alginate embedded magnetic nanoheaters: A combined therapy. *Adv. Mater.* **2011**, *23*, 787–790.

15. Liang, Y., Zhang, L.M.; Jiang, W.; Lei, W. Embedding magnetic nanoparticles into polysaccharide-based hydrogels for magnetically assisted bioseparation. *Chem. Phys. Chem.* **2007**, *8*, 2367–2372.

16. Liu, H.; Wang, C.; Gao, Q.; Chen, J.; Ren, B.; Liu, X.; Tong, Z. Facile fabrication of well-defined hydrogel beads with magnetic nanocomposite shells. *Int. J. Pharm.* **2009**, *376*, 92–98.

17. Pasqui, D.; Atrei, A.; Giani, G.; de Cagna, M.; Barbucci, R.; Metal oxide nanoparticles as cross-linkers in polymeric hybrid hydrogels. *Mater. Lett.* **2011,** *65*, 392–395.

18. Shin, K.; Cho,Y.; Choi, J.; Kim, K. Facile synthesis of silver-deposited silanized magnetite nanoparticles and their application for catalytic reduction of nitrophenols. *Appl. Catal. A Gen.* **2012**. In press.

19. Berghoute, Y.; Mendonc, M.H.; Hamdani, M.; Pereira, M.I.S. Electrochemical behaviour of FexCo$_3$−xO$_4$ with (x = 0, 1, 2 and 3) oxides thin film electrodes in alkaline medium. *J. Appl. Electrochem.* **2009**, *39*, 2469–2479.

20. Laouini, E.; Douch, J.; Hamdani, M.; Berghoute, Y.; Mendonc, M.H.; Pereira, M.I.S.; Singht, R.N. Cathodic behaviour of CoFe$_2$O$_4$ spinel electrodes in alkaline medium. *J. Appl. Electrochem.* **2011**, *41*, 731–740.

21. Choi, Y.J.; Tzy-Jiun, U.; Luo, M. Sol-gel chemistry of an aqueous precursor solution for YBCO thin films. *J. Sol-Gel. Sci. Technol.* **2009**, *51*,124–133.

22. Hernando J.; Pourrostami, T.; Garrido, J.A.; Williams, O.A.; Gruen, D.M.; Kromka, A.; Steinmüller, D.; Stutzmann, M. Immobilization of horseradish peroxidase via an amino silane on oxidized ultrananocrystalline diamond. *Diamond Relat. Mater.* **2007**, *16*, 138–143.

23. Wang, M.; Liechti, K.M.; Wang, Q.; White, J.M. Self-assembled silane monolayers: Fabrication with nanoscale uniformity. *Langmuir* **2005**, *21*, 1848–1857.

24. Moon, J.H.; Shin, J.W.; Kim, S.Y.; J. W. Park formation of uniform aminosilane thin layers: An imine formation to measure relative surface density of the amine group. *Langmuir* **1996**, *12*, 4621–4624.

25. Pallandre, A.; Glinel, K.; Jonas, A.M.; Nysten, B. Binary nanopatterned surfaces prepared from siane monolayers. *Nanoletters* **2004**, *4*, 365–371.

26. Kurth, D.G.; Bein, T. Surface reactions on thin layers of silane coupling agents. *Langmuir* **1993**, *9*, 2965–2973.

27. Xu, R. Progress in nanoparticles characterization: Sizing and zeta potential measurement. *Particuology* **2008**, *6*, 112–115.

28. Rodríguez-Arco, L.; López-López, M.; González-Caballero, F.; Durán, J. Steric repulsion as a way to achieve the required stability for the preparation of ionic liquid-based ferrofluids. *J. Colloid Interf. Sci.* **2011**, *357*, 252–254.

29. Bihari, P.; Vippola, M.; Schultes, S.; Praetner, M.; Khandoga, A.; Reichel, C.; Coester, C.; Tuomi, T.; Rehbergand, M.; Krombach, F. Optimized dispersion of nanoparticles for biological *in vitro* and *in vivo* studies. *Part. Fibre Toxicol.* **2008**, *5*, doi:10.1186/1743-8977-5-14. Avaliable online: http://www.ncbi.nlm.nih.gov/pmc/articles/PMC2584664/ (accessed on 28 April 2012).

30. Zhang, X.; Yin, L.; Tang, M.; Pu, Y. Optimized method for preparation of TiO_2 nanoparticles dispersion for biological study. *J. Nanosci. Nanotechnol.* **2010**, *10*, 5213–5219.

31. Vargas, A.F.; Orozco, V.H.; Rault, F.; Giraud, S.; Devaux, E.; Lopez B. L. Influence of fiber-like nanofillers on the rheological, mechanical, thermal and fire properties of polypropylene: An application to multifilament yarn. *Compos. Part. A Appl. Sci. Manuf.* **2010**, *41*, 1797–1806.

32. Tjong, S.C. Structural and mechanical properties of polymer nanocomposites. *Mater. Sci. Eng. Rep.* **2006**, *53*, 73–197.

33. Hu, X.; Zhou, J.; Zhang, N.; Tan, H.; Gao, C. Preparation and properties of an injectable scaffold of poly(lactic-co-glycolic acid) microparticles/chitosan hydrogel. *J. Mech. Behav.* **2008**, *1*, 352–359.